Dislocation-Stacking Fault Tetrahedron Interactions in Cu

B. D. Wirth[1]

V. V. Bulatov

T. Diaz de la Rubia

Chemistry and Materials Science Directorate,
Lawrence Livermore National Laboratory,
Livermore, CA 94550

In copper and other face centered cubic metals, high-energy particle irradiation produces hardening and shear localization. Post-irradiation microstructural examination in Cu reveals that irradiation has produced a high number density of nanometer sized stacking fault tetrahedra. The resultant irradiation hardening and shear localization is commonly attributed to the interaction between stacking fault tetrahedra and mobile dislocations, although the mechanism of this interaction is unknown. In this work, we present results from a molecular dynamics simulation study to characterize the motion and velocity of edge dislocations at high strain rate and the interaction and fate of the moving edge dislocation with stacking fault tetrahedra in Cu using an EAM interatomic potential. The results show that a perfect SFT acts as a hard obstacle for dislocation motion and, although the SFT is sheared by the dislocation passage, it remains largely intact. However, our simulations show that an overlapping, truncated SFT is absorbed by the passage of an edge dislocation, resulting in dislocation climb and the formation of a pair of less mobile super-jogs on the dislocation. [DOI: 10.1115/1.1479692]

Introduction

It is well established that irradiation of metals by high-energy neutrons and ions produces significant changes in material microstructure and mechanical properties [1–5]. In low stacking fault energy, face centered cubic (fcc) metals, stacking fault tetrahedra (SFT) are the primary defect observed following high-energy particle irradiation. For example, post-irradiation microstructural examination of copper irradiated at temperatures between 20 and 100°C and doses between 10^{-4} and 10^{2} dpa reveals that approximately 90% of the high number density (about 10^{23} m^{-3}) of radiation-induced defects are SFTs and that the average SFT size remains constant at about 2.5 ± 0.5 nm [3,6].

When deformed after irradiation, Cu and other low stacking fault energy fcc metals exhibit significant mechanical property degradation, including a sharp increase in yield stress, a decrease in ductility and often, plastic flow localization in the form of defect-free dislocation channels [2,5]. The formation of dislocation channels is commonly attributed to dislocation absorption of the vacancies contained in SFTs [7,8]. However, a concise atomistic picture of the SFT absorption mechanism is lacking. Thus, the objective of this work is to obtain atomistic insight into the interaction of SFTs with dislocations, necessary to understand radiation-induced mechanical property changes.

Atomistic simulations can provide significant insight into the mechanisms of dislocation motion and interaction with defect clusters at high strain rates. Such insight is of practical importance for developing quantitative structure-property relationships, mechanistic understanding of plastic flow localization and predictive models of mechanical behavior in metals under irradiation. Computer simulation studies have been used to successfully model the production and accumulation of damage in irradiated Cu [8–15], as well as the interaction between dislocations and self-interstitial clusters in Ni [16]. Some key results of our work, focused on the dominant defects produced in irradiated Cu, are briefly summarized here. Molecular dynamics (MD) simulations of displacement cascade evolution in Cu reveal the formation of large vacancy and self-interstitial loops [8–12]. The self-interstitial cluster loops undergo easy, one-dimensional transport [13] and are assumed to rapidly migrate away from the vacancy rich cascade region. The clustered vacancies then collapse to form SFTs, which occurs within a few picoseconds at room temperature by a dislocation mechanism [14], consistent with that first proposed by Silcox and Hirsch [17]. Interestingly, a number of MD simulations predict that the SFT structure will not consist of perfect tetrahedron, but in most cases, will actually consist of truncated tetrahedron [14,18] and in some cases, overlapping, truncated SFTs[2] [14].

In this paper, we will present some of our recent MD simulation results to understand the mobility of edge dislocations in Cu at high strain rate and their interactions with the principle defects observed under neutron irradiation, namely, stacking fault tetrahedron and overlapping, truncated stacking fault tetrahedra.

Simulation Methodology

MD simulations of the interaction and fate of moving edge dislocations in Cu were performed using the MDCASK code [19] and an embedded atom method (EAM) potential [20,21]. The elastic constants and stacking fault energy obtained with the EAM potential are provided in Table 1. It is important to mention that the EAM potential used in this work gives a very low stacking fault energy compared to experimental values. At present, it is not entirely clear what effect the low stacking fault energy has on the simulation results reported here. Additional simulations are now being performed with an EAM potential that gives a more realistic value of the stacking fault energy and will be reported in a future publication.

The simulations were performed in a cubic cell bounded by $\langle 111 \rangle$, $\langle 110 \rangle$ and $\langle 112 \rangle$ faces, as sketched in Fig. 1. Periodic boundary conditions are applied in the $Y=[110]$ and $Z=[\bar{1}12]$ directions, while the $X=[\bar{1}11]$ faces are free surfaces during equilibration at 100 K and then traction controlled with a constant applied force.

An edge dislocation is introduced in the simulation cell by removing two (220) half-planes and equilibrating the system at 100 K to allow the edge dislocation, $\mathbf{b}=a/2\langle 110 \rangle (111)$, to split into two Shockley partial dislocations, $\mathbf{b}=a/6\langle 112 \rangle (111)$, separated

[1]Corresponding author. Contact information: phone (925) 424-9822, fax (925) 423-7040, wirth4@llnl.gov.

Contributed by the Materials Division for publication in the JOURNAL OF ENGINEERING MATERIALS AND TECHNOLOGY. Manuscript received by the Materials Division November 2, 2001; revised manuscript received March 6, 2002. Guest Editors: Tariq A. Khraishi and Hussein M. Zbib.

[2]A triangular vacancy platelet on a {111} plane bounded by three $\langle 110 \rangle$ directions forms a single SFT. A triangular vacancy platelet bounded by two $\langle 110 \rangle$ and one $\langle 112 \rangle$ directions forms two partial (truncated) SFTs, one above and one below the initial plane; we define this as an overlapping truncated SFT.

Table 1 Elastic constants (c_{11}, c_{12}, c_{44} and shear modulus, μ) and stacking fault energy obtained from the EAM Cu potential [17,18] used in this work

C_{11}	176 GPa
C_{12}	129 GPa
C_{44}	82.3 GPa
μ	58.8 GPa
Stacking fault energy	11.4 mJ/m^2

by a stacking fault. SFT and overlapping, truncated SFTs were also inserted into the simulation cell on the $(\bar{1}11)$ glide plane ahead of the dissociated edge dislocation.

Following equilibration at 100 K, a constant shear stress, τ_{yx}, is applied by superimposing a constant force in the [110] direction on the atoms in the two $(\bar{1}11)$ surfaces. In the results reported here, the simulation cell was 31.2 nm in *X*, 25.5 nm in *Y* and either 14.0 or 38.8 nm in *Z* (along the dislocation line), which corresponds to a dislocation density of about 8×10^{14} m^{-2} and a SFT density of 3 to 9×10^{22} m^{-3}. Simulations have been performed using cells of different size and dimension, but have not resulted in any qualitative difference from the results described here. The dislocation and SFT are visualized by plotting the location of atoms with high potential energy.

Results and Discussion

Figure 2 shows a series of MD simulation snapshots of the $(\bar{1}11)$ glide plane (in $[\bar{1}\bar{1}1]$ projection) of the motion of an isolated edge dislocation under stress of 300 MPa at 100 K. The edge dislocation is noticeably split into two Shockley partial dislocations, with a mean separation of ~8.5 nm. This large value of the equilibrium separation results from the very low value of the stacking fault energy of this Cu EAM potential, as shown in Table 1, relative to experimental values of 30–45 mJ/m^2. Approximately 5 ps after application of the applied stress, the partial dislocations begin to move, and pass through the cell many times as they quickly reach a steady velocity. The motion of the leading partial through the periodic boundaries occurs between 15 and 20.5 ps, as shown in Figs. 2(*c*) and 2(*d*). To date, the motion and steady state velocity of dissociated edge dislocations have been measured from the MD simulations for applied stresses between 45 and 375 MPa.

Figure 3 shows the steady state velocity of an isolated edge dislocation obtained from the computer simulations. It is important to note that, as a consequence of the periodic boundary conditions, the dislocation is not actually isolated, but the simulations are performed for an array of infinitely straight edge dislocations with a mean spacing of 25.5 nm, which corresponds to a dislocation density of about 8×10^{14} m^{-2}. The results show an apparent saturation in steady state velocity of about 1500 m/s for applied stresses above about 200 MPa, which corresponds to a strain rate of $\sim3\times10^{8}$ s^{-1}. The saturation velocity is about 55% of the calculated transverse shear wave speed of ~2800 m/s for this Cu EAM potential. As reported in Ref. [16], the saturation velocity depends on the applied boundary conditions. Our value of ~55% agrees well with the value of ~59% obtained by Rodney and Martin for edge dislocation saturation velocity in Ni, with comparable boundary conditions [16]. Simulations are currently in progress to extend the simulations of dislocation mobility to higher applied stresses.

Figure 4 shows a series of MD simulation snapshots of the $(\bar{1}11)$ glide plane (in $[\bar{1}11]$ projection) of the interaction between a moving, dissociated edge dislocation and a perfect SFT, whose

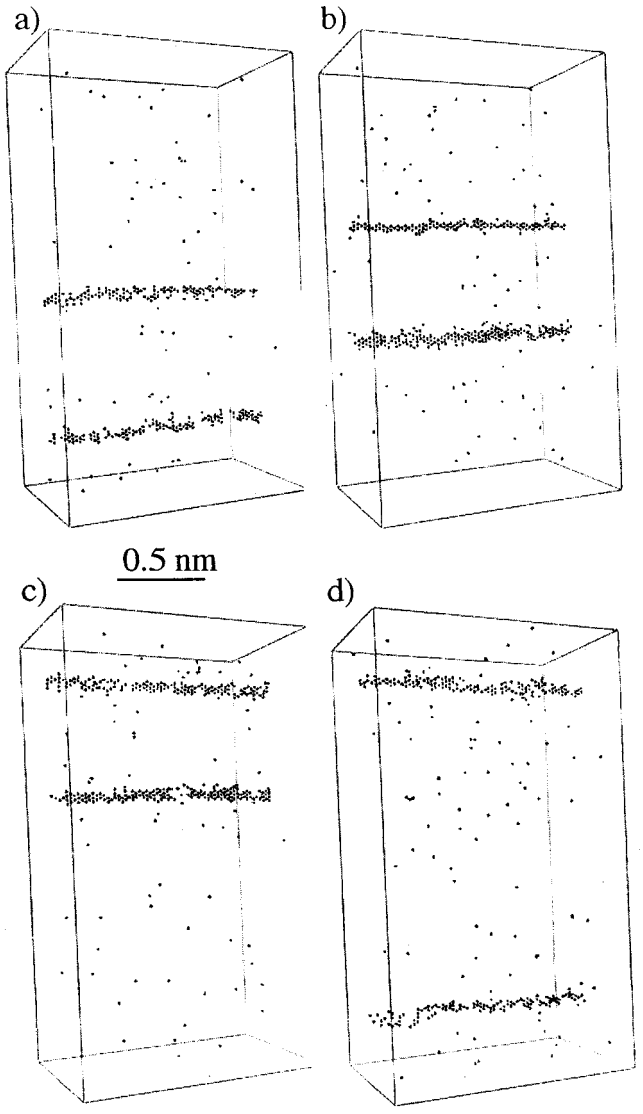

Fig. 2 Near $[\bar{1}\bar{1}1]$ projection of MD simulation snapshots showing the motion of an isolated edge dislocation. The dislocation is visualized by plotting atoms with high potential energy. Dislocation positions are shown at (*a*) 0.0 ps, (*b*) 7.0 ps, (*c*) 15.0 ps, and (*d*) 20.5 ps after applying a 300 MPa shear stress.

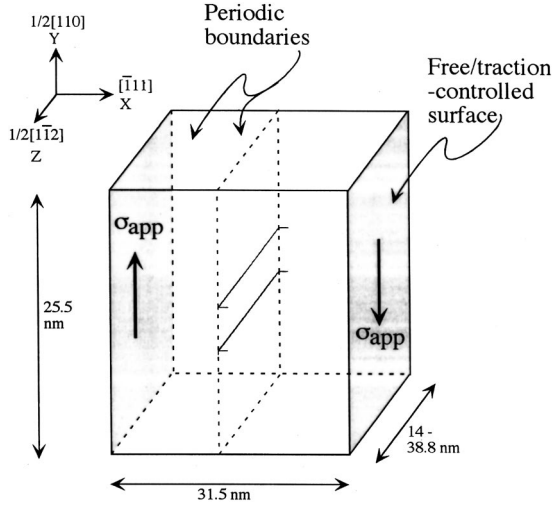

Fig. 1 Schematic view of the simulation cell and dimensions used in this work

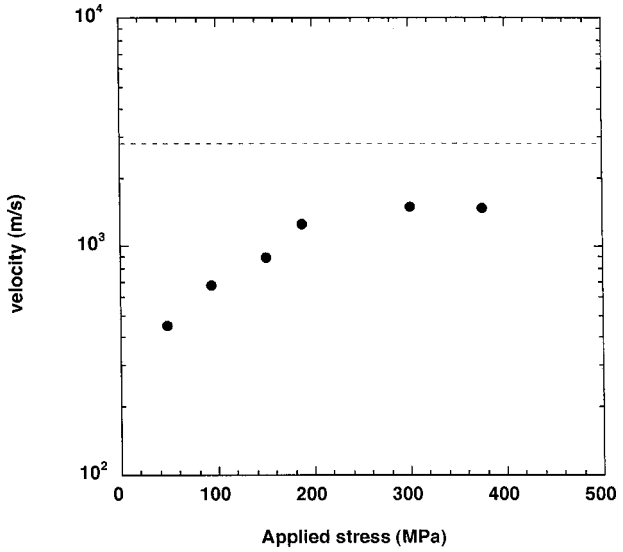

Fig. 3 Steady-state velocity of an edge dislocation as a function of the applied shear stress

base lies on the dislocation glide plane. The simulation was performed at an initial temperature of 100 K and an applied shear stress of 300 MPa. Figure 4(*a*) shows the initial configuration of the edge dislocation, which is split into the two Shockley partial dislocations, and the SFT, which consists of 6 stair-rod dislocations when viewed using high potential energy atoms. Although not seen in this projection, the base of the SFT lies just above the glide plane of the edge dislocation. Following application of the shear stress, the two Shockley partial dislocations are driven towards the SFT. Figure 4(*b*) shows the position of the partial dislocations 9 ps after application of the 300 MPa shear stress. By this time, the leading Shockley partial dislocation has reached the SFT, felt a repulsive force and bowed back away from the SFT. As the trailing partial approaches, the leading partial slips past the SFT base (Fig. 4(*c*)). The SFT acts as a hard barrier to dislocation motion and in order for the leading partial to shear past the SFT, it must noticeably bow around it, finally releasing at a critical angle of about 80 deg (Fig. 4(*d*)). By 15.5 ps (Fig. 4(*e*)) the trailing partial shears the SFT, as the leading partial continues to move ahead with significant remaining curvature along its line. Interestingly, the SFT provides less resistance to the passage of the trailing partial and the shape of the trailing partial shows only a slight perturbation immediately after passing the SFT (Fig. 4(*f*)). The

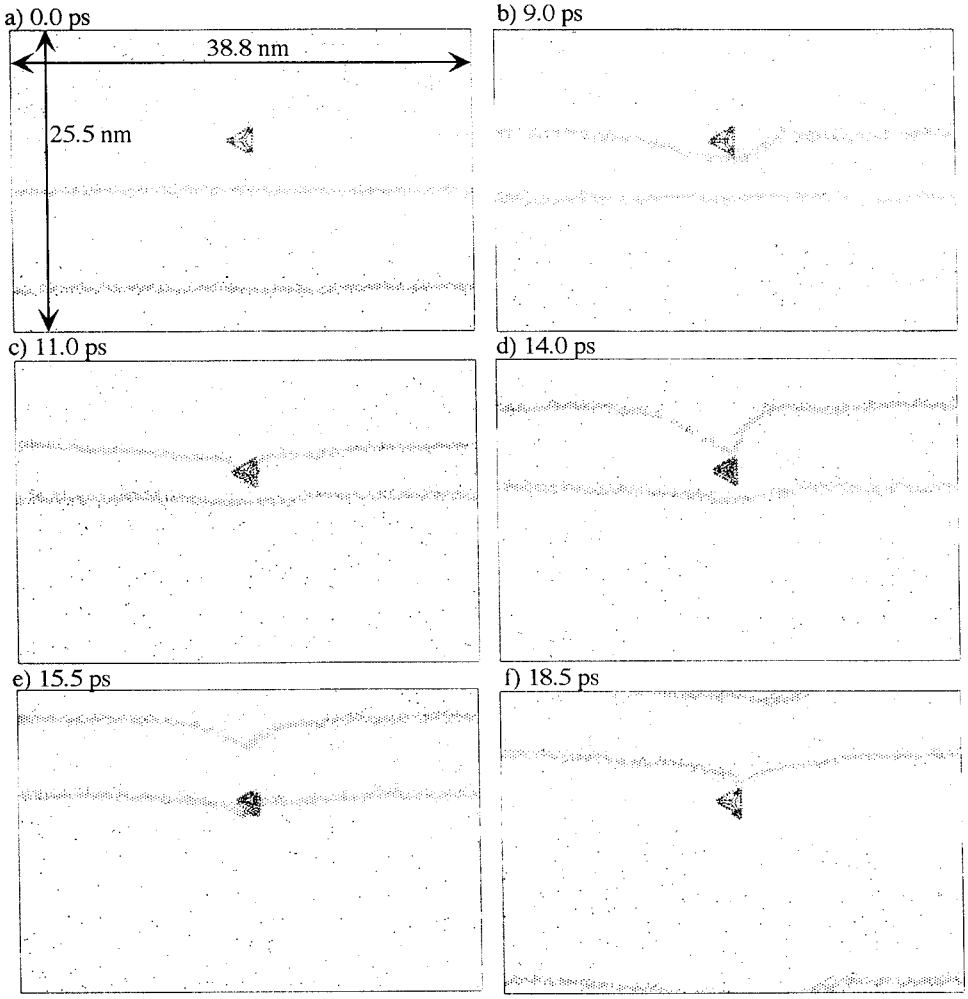

Fig. 4 $[\bar{1}11]$ projection of MD simulation snapshots showing the interaction between a moving, dissociated edge dislocation and an SFT, whose base lies just above the dislocation glide plane, as visualized by plotting atoms with high potential energy. Dislocation positions are shown at (*a*) 0.0 ps, (*b*) 9.0 ps, (*c*) 11.0 ps, (*d*) 14.0 ps, (*e*) 15.5 ps, and (*f*) 18.5 ps after applying a 300 MPa shear stress. Note, the use of high potential energy atoms for visualization introduces thermal noise (isolated points) into the snapshots.

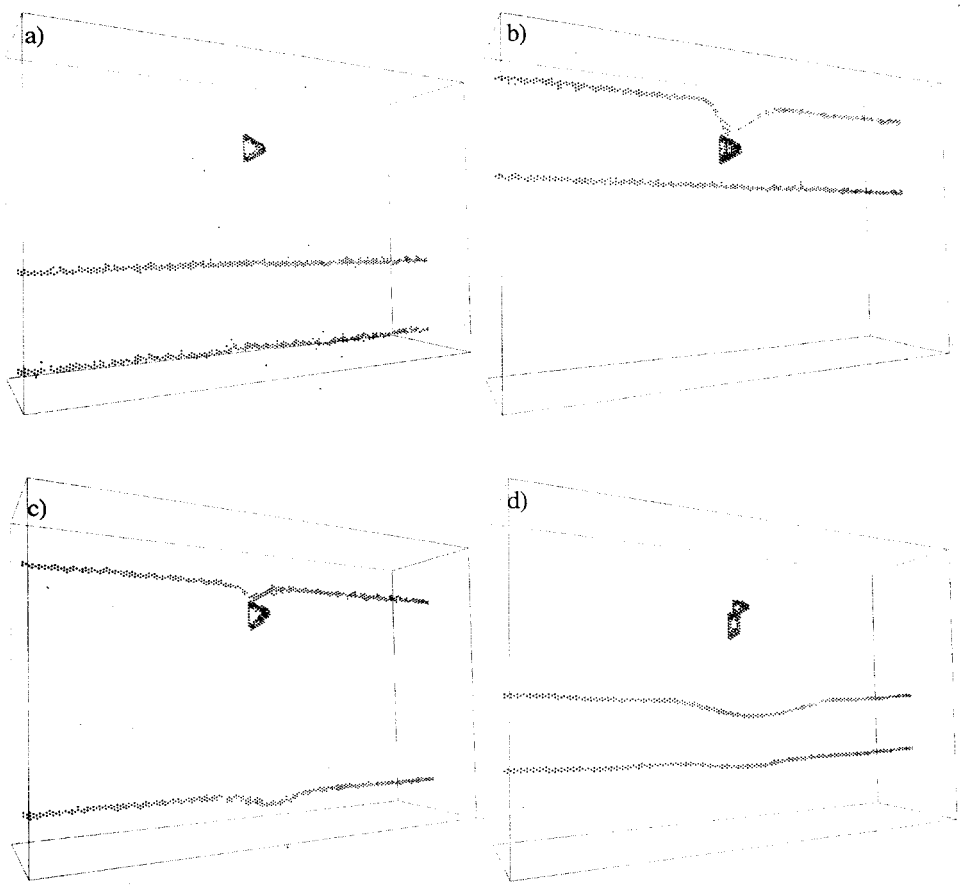

Fig. 5 Near [$\bar{1}\bar{1}1$] projection of MD simulation snapshots showing the interaction between a moving, dissociated edge dislocation and an SFT which lies across the dislocation glide plane, as visualized by plotting atoms with high potential energy. Dislocation positions are shown at (*a*) 10.0 ps, (*b*) 19.5 ps, (*c*) 23.3 ps, and (*d*) 115.0 ps after applying a 300 MPa shear stress. Note, the edge dislocation has passed through the SFT six times, shearing the top portion of the SFT away from its truncated tetrahedron base.

SFT is not absorbed by the moving edge dislocation, but instead acts as a rather hard obstacle to dislocation motion. In this case, with the dislocation shearing the perfect SFT, with its base on the dislocation glide plane, the entire SFT is sheared by a complete Burgers vector ($a/2\langle 110\rangle$) by the passage of the edge dislocation.

Figure 5 shows a series of MD simulation snapshots of the ($\bar{1}\bar{1}1$) glide plane (in near [$\bar{1}\bar{1}1$] projection) of the interaction between a moving, dissociated edge dislocation and a perfect SFT, which lies across the dislocation glide plane. Again, the simulation was performed at an initial temperature of 100 K and an applied stress of 300 MPa. Figure 5(*a*) shows the configuration of the edge dislocation, which is split into the two Schockley partial dislocations, and the SFT, which in this case lies across the dislocation glide plane, 10.0 ps after applying the shear stress. Figure 5(*b*) shows the position of the leading and partial dislocations 19.5 ps after applying the 300 MPa shear stress. By this time, the leading partial has just by-passed the SFT, producing a shear of $a/6\langle 112\rangle$ in the portion of the SFT which lies above the glide plane. Again, the SFT acts as a hard, shearable obstacle and the critical angle of the leading partial immediately after it bypasses the SFT is ~80 deg. The trailing partial shears through the SFT 23.3 ps after applying the shear stress, and again, the SFT offers significantly less resistance to the trailing partial, shown in Fig. 5(*c*). This simulation was run for longer times to allow the dislocation to pass through the SFT five additional times. Notably, the SFT was neither destroyed nor absorbed, but although considerably sheared, as shown in Fig. 5(*d*), was largely intact.

Following each passage of the dislocation through the SFT, the portion of the SFT lying above the dislocation glide plane is sheared by a Burgers vector, and thus has a surface step (ledge) along three of its four {111} faces, but remains largely intact. Qualitatively similar results are observed in simulations of the edge dislocation-SFT interaction performed with a range of applied stress from 50 to 300 MPa, different SFT separation along the dislocation line and slightly different interaction geometry. In all cases, the SFT acts as a hard barrier and despite the formation of surface steps, remains intact following dislocation passage. Indeed, as shown in Fig. 5(*d*) even after 6 dislocations have sheared the SFT it remains largely intact, albeit with further dislocation passage, it will ultimately be separated into a small perfect SFT near a truncated tetrahedron base.

However, dislocation absorption of an SFT-type defect has been observed in the case where the SFT is not perfect, but rather consists of overlapping, truncated SFTs. As mentioned previously, overlapping, truncated SFTs are the predicted defect from MD/KMC simulations of damage accumulation under irradiation [13]. Figure 6 shows the results of a simulation between a dissociated edge dislocation and overlapping, truncated SFT at 100 K in Cu. In this simulation, an overlapping, truncated SFT, with a spacing of 14 nm (along the dislocation line), is placed on the glide plane of a dissociated edge dislocation, which moves under an applied shear stress of 300 MPa. Figure 6(*a*) shows the initial configuration of the edge dislocation, split into two Shockley partial dislocations, and the overlapping, truncated SFT (most easily visual-

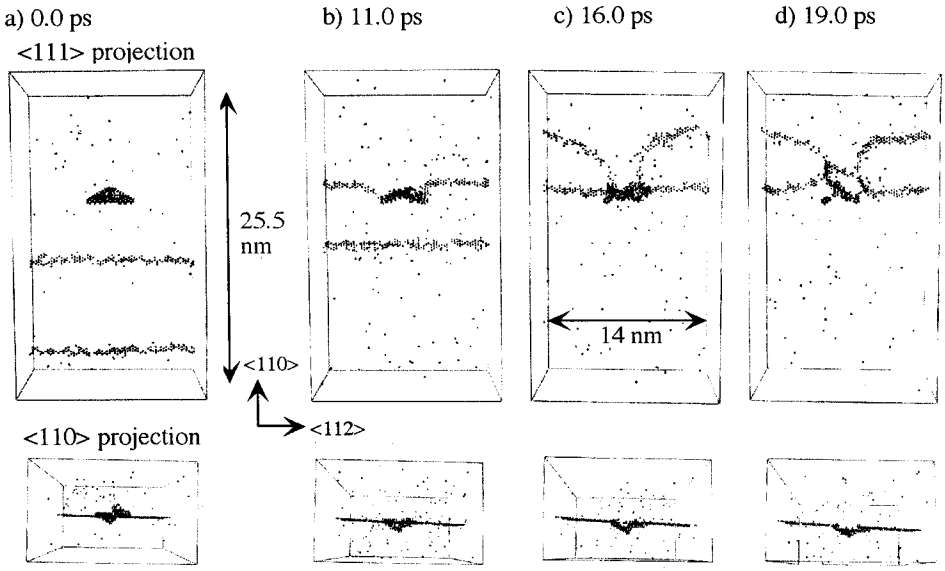

Fig. 6 MD simulation snapshots showing the interaction between a moving, dissociated edge dislocation and an overlapping, truncated SFT in Cu. The high potential energy atoms are visualized in ⟨111⟩ (top) and ⟨110⟩ (bottom) projections and show the motion of the two Shockley partials and interaction with the overlapping, truncated SFT at (*a*) 0, (*b*) 11.0, (*c*) 16.0, and (*d*) 19.0 ps after application of a 300 MPa shear stress. See text for additional details.

ized in ⟨110⟩ projection), as represented through visualization of the atoms with high potential energy. Figure 6(b) shows that upon contact, the leading partial absorbs vacancies from part of the overlapping truncated SFT and climbs, forming a pair of superjogs that effectively pin the leading partial as the trailing partial approaches. Figure 6(*c*) shows that the trailing partial catches the leading partial at the location of the overlapping SFT and superjog pair, climbs through absorption of the remaining vacancies in the defect and constricts at the location of the superjogs. Following defect absorption, the dislocation continues to move (Fig. 6(d)), but with a decreased mobility associated with the superjogs.

The detailed absorption mechanism is complicated and has not yet been completely analyzed. It is clear that passage of a single dislocation through a perfect SFT will not lead to its absorption, but it is not yet known how many dislocations are required to completely shear a SFT, or what degree of SFT truncation will result in absorption. However, it is clear that defect absorption produces dislocation climb and the formation of superjog pairs, which have decreased mobility. Similar dislocation climb behavior resulting from defect absorption was observed by Rodney and Martin in the absorption of self-interstitial clusters in Ni [16]. In that case, the dislocation climbed in the opposite direction from the absorption of vacancies from the overlapping, truncated SFT reported here. In both cases, one of the superjogs is initially constricted, presumably in the form of a Lomer segment, as discussed by Rodney and Martin [16]. The constricted superjog is essentially sessile, but can transform to a more favorable (glissile) configuration through the incorporation of three self-interstitials, as discussed in Ref. [16]. This process occurred just prior to the snapshot shown in Fig. 6(*c*), and indeed, the small cluster of high energy atoms seen below the left superjog in Fig. 6(*d*) has been identified to consist of three vacancies.

Conclusions

MD simulation results have been presented of the steady state velocity of 'isolated' edge dislocations and the interaction between a moving edge dislocation and stacking fault tetrahedra at high strain rates. The results show that a perfect SFT acts as a relatively hard obstacle for dislocation motion and, although the SFT is sheared by the dislocation passage, it remains largely intact. However, our simulations show that an overlapping, truncated SFT is absorbed by the passage of an edge dislocation, resulting in dislocation climb and the formation of a pair of less mobile super-jogs on the dislocation. Additional simulations are underway to characterize the matrix of possible dislocation-SFT interactions, including the effect of applied stress and the use of another EAM potential to determine the effect of stacking fault energy, and provide rules for dislocation dynamics simulations that can provide insight into the mechanisms responsible for flow localization in irradiated metals.

Acknowledgment

This work was performed under the auspices of the U.S. Department of Energy by University of California Lawrence Livermore National Laboratory under contract No. W-7405-Eng-48.

References

[1] Mansur, L. K., and Bloom, E. E., 1982, "Radiation Effects in Reactor Structural Alloys," J. Met., **34**, pp. 23–31.
[2] Lucas, G. E., 1993, "The Evolution of Mechanical Property Change in Irradiated Austenitic Stainless Steels," J. Nucl. Mater., **206**, pp. 287–305.
[3] Singh, B. N., and Zinkle, S. J., 1993, "Defect Accumulation in Pure FCC Metals in the Transient Regime: A Review," J. Nucl. Mater., **206**, pp. 212–229.
[4] Trinkaus, H., Singh, B. N., and Foreman, A. J. E., 1997, "Segregation of Cascade Induced Interstitial Loops at Dislocations: Possible Effect on Initiation of Plastic Deformation," J. Nucl. Mater., **251**, pp. 172–187.
[5] Victoria, M., Baluc, N., Bailat, C., Dai, Y., Luppo, M. I., Schaublin, R., and Singh, B. N., 2000, "The Microstructure and Associated Tensile Properties of Irradiated FCC and BCC Metals," J. Nucl. Mater., **276**, pp. 114–122.
[6] Dai, Y., and Victoria, M., 1997, "Defect Cluster Structure and Tensile Properties of Copper Single Crystals Irradiated With 600 MeV Protons," Mat. Res. Soc. Symp. Proc., Vol. 439, pp. 319–324.
[7] Ghoniem, N. M., Tong, S.-S., and Sun, L. Z., 2000, "Parametric Dislocation Dynamics: A Thermodynamics-Based Approach to Investigations of Mesoscopic Plastic Deformation," Phys. Rev. B, **139**(1), pp. 913–927.
[8] Diaz de la Rubia, T., Zbib, H. M., Khraishi, T. A., Wirth, B. D., Victoria, M., and Caturla, M. J., 2000, "Plastic Flow Localization in Irradiated Materials: A Multiscale Modeling Approach," Nature (London), **406**, pp. 871–874.
[9] Wirth, B. D., Caturla, M. J., Diaz de la Rubia, T., Khraishi, T., and Zbib, H., 2001, "Mechanical Property Degradation in Irradiated Materials: A Multiscale Modeling Approach," Nuclear Instruments and Methods B, **180**, pp. 23–31.
[10] Diaz de la Rubia, T., and Guinan, M. W., 1992, "New Mechanism of Defect Production in Metals: a Molecular-Dynamics Study of Interstitial-Dislocation-

Loop Formation in High-Energy Displacement Cascades,'' Phys. Rev. Lett., **66**, pp. 2766–2769.
[11] Phythian, W. J., Stoller, R. E., Foreman, A. J. E., Calder, A. F., and Bacon, D. J., 1995, ''A Comparison of Displacement Cascades in Copper and Iron by Molecular Dynamics and Its Application to Microstructural Evolution,'' J. Nucl. Mater., **223**, pp. 245–261.
[12] Averback, R. S., and Diaz de la Rubia, T., 1998, ''Displacement Damage in Irradiated Metals and Semiconductors,'' Solid State Phys., **51**, pp. 281–402.
[13] Osetsky, Y. N., Bacon, D. J., Serra, A., Singh, B. N., and Golubov, S. I. Y., 2000, ''Stability and Mobility of Defect Clusters and Dislocation Loops in Metals,'' J. Nucl. Mater., **276**, pp. 65–77.
[14] Wirth, B. D., Bulatov, V., and Diaz de la Rubia, T., 2000, ''Atomistic Simulation of Stacking Fault Tetrahedra Formation in Cu,'' J. Nucl. Mater., **283–287**, pp. 773–777.
[15] Caturla, M. J., Soneda, N., Alonso, E. A., Wirth, B. D., and Diaz de la Rubia, T., 2000, ''Comparative Study of Radiation Damage Accumulation in Cu and Fe.'' J. Nucl. Mater., **276**, pp. 13–21.
[16] Rodney, D., and Martin, G., 2000, ''Dislocation Pinning by Glissile Interstitial Loops in a Nickel Crystal: A Molecular-Dynamics Study,'' Phys. Rev. B, **61**, pp. 8714–8725.
[17] Silcox, J., and Hirsch, P. B., 1959, ''Direct Observations of Defects in Quenched Gold,'' Philos. Mag., **4**, pp. 72–89.
[18] Osetsky, Y. N., and Bacon, D. J., 2001, ''Defect Cluster Formation in Displacement Cascades in Copper,'' Nuclear Instruments and Methods B, **180**, pp. 85–90.
[19] Diaz de la Rubia, T., and Guinan, M. W., 1990, ''Progress in The Development of a Molecular Dynamics Code for High-Energy Cascade Studies,'' J. Nucl. Mater., **174**, pp. 151–157.
[20] Foiles, S. M., Baskes, M. I., and Daw, M. S., 1986, ''Embedded-Atom-Method Functions for the FCC Metals Cu, Ag, Au, Ni, Pd, Pt, and Their Alloys,'' Phys. Rev. B, **33**, pp. 7983–7991.
[21] M. Ghaly and R. S. Averback, personal communication.